Frozen orbits for Lunar Satellites

Christos Efthymiopoulos

Department of Physics – Aristotle University of Thessaloniki

CELMEC-IX – The Ninth International Meeting on Celestial Mechanics (2026)

The double origin of frozen orbits

Example: the Earth's satellite orbits $H = H_{Kep} + H_{J_2}^{(av)} + H_{J_3}^{(av)} + H_{J_4}^{(av)} + H_{J_2^2}^{(av)} + H_{TB}$

$$H_{J_2}^{(av)} = -J_2 \frac{\mu_E}{a^3(1-e^2)^{3/2}}\left(\frac{1}{2} - \frac{3}{4}\sin^2 i\right)$$

$$\mathcal{H}_{J_3}^{(av)} = J_3 \frac{3\mu_E R_E^3 e \sin i}{2a^4(1-e^2)^{5/2}}\left(1 - \frac{5}{4}\sin^2 i\right)\sin(g)$$

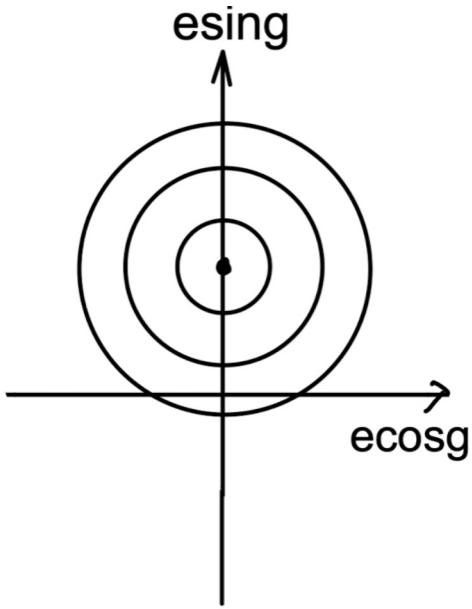
$$\mathcal{H}_{J_4}^{(av)} = J_4 \frac{3\mu_E R_E^4}{8a^5(1-e^2)^{7/2}}\left(-1 - \frac{3e^2}{2} + \left(5 + \frac{15e^2}{2}\right)\sin^2 i - \frac{35}{8}\left(1 + \frac{3e^2}{2}\right)\sin^4 i - \frac{15e^2\sin^2 i}{4}\left(1 - \frac{3\sin^2 i}{2}\right)\cos(2g)\right),$$

$$\mathcal{H}_{J_2^2}^{(av)} = -J_2^2 \frac{3\mu_E R_E^4}{8a^5(1-e^2)^{7/2}}\left[\frac{5}{2} + \eta - \frac{1}{2}\eta^2 - \left(5 + 3\eta - \frac{1}{2}\eta^2\right)\sin^2 i + \left(\frac{35}{16} + \frac{9}{4}\eta + \frac{5}{16}\eta^2\right)\sin^4 i - \left(\left(\frac{15}{4}(1+\eta) - \frac{23}{4}\eta^2 - \frac{7}{4}\eta^3\right)\sin^2 i + \left(-\frac{35}{8}(1+\eta) + \frac{55}{8}\eta^2 + \frac{15}{8}\eta^3\right)\sin^4 i\right)\frac{\cos(2g)}{1+\eta}\right]$$

with $\eta = \sqrt{1-e^2}$.

Frozen orbits: heuristic definition

$$\dot{g} \approx 0, , \dot{e} \approx 0$$



Frozen orbits at (and around) the forced equilibrium

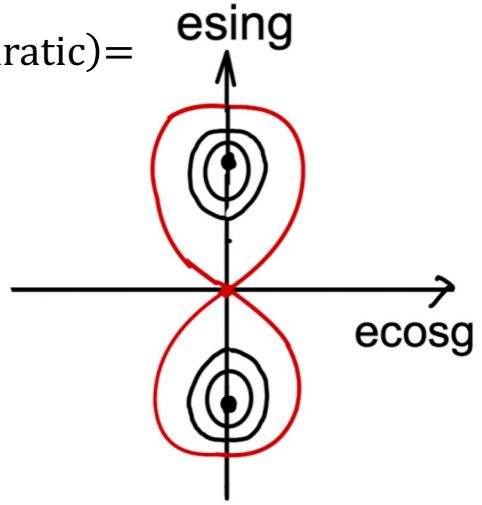
Example: J2+J3 at LEO

$$c_1(a,i)e^2(x^2+y^2, \text{unperturbed}) + c_2(a,i)e \sin g(y, \text{linear})$$

Frozen orbits by the Lidov-Kozai mechanism

Example: J_2+J_4 + J_2^2 + Moon

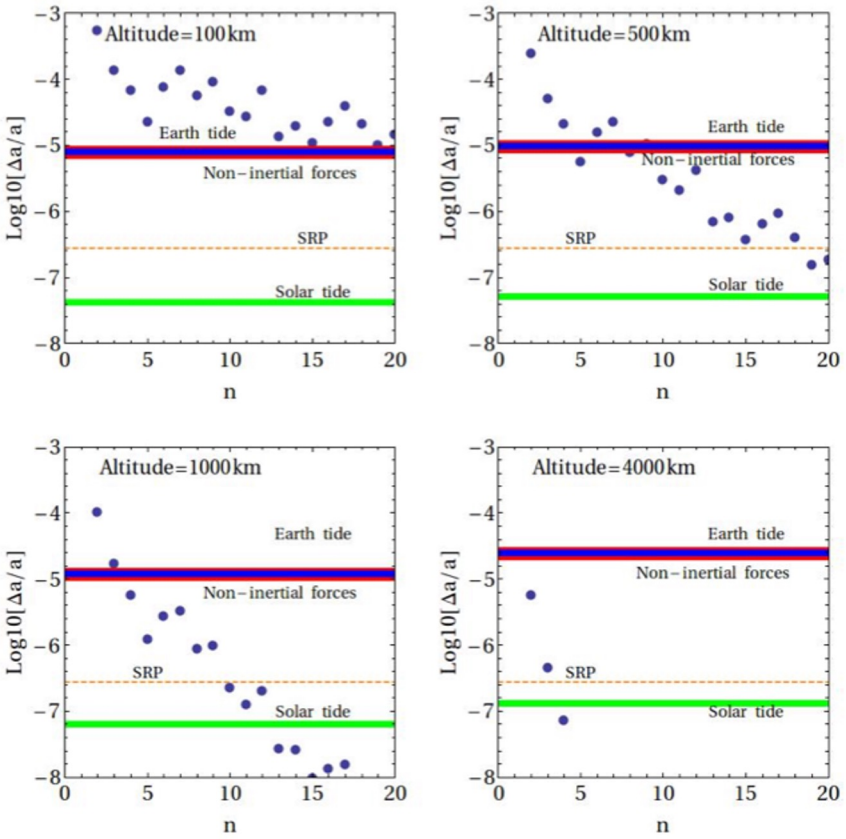
$$c_1(a,i)e^2(x^2+y^2, \text{unperturbed}) + c_2(a,i)e^2\cos(2g)(x^2-y^2, \text{quadratic}) = (c_1+c_2)x^2 + (c_1-c_2)y^2 + O(e^4)$$



As the altitude increases, the J_4 + J_2^2 terms compete with the Moon's tidal terms (Moon gives the dominant contribution at altitudes beyond ≈ 2 Earth radii)

$$\text{Moon's term (averaged)} \approx -\frac{9\mu_E a^2 \sin^2(i) e^2}{16 a_{Moon}^3}\cos(2g)$$

Complexity of the problem for Moon-orbiting satellites





SELENA Propagator (2022)
(C.E (UniPD) - K. Tsiganis, I. Gkolias – M. Gaitanas (AUTh), C. Yanez (CNES)

$$\frac{\Delta a(n)}{a_{Kep}} \sim \sum_{m=0}^{n} \frac{(n+1)R_{\leftmoon}^{n}}{r^{n}} \left(C_{nm}^{2} + S_{nm}^{2}\right)^{1/2}$$

$$\frac{\Delta a_{\oplus}}{a_{Kep}} \sim \frac{M_{\oplus} r^{3}}{M_{\leftmoon} a_{\oplus}^{3}}, \qquad \frac{\Delta a_{\odot}}{a_{Kep}} \sim \frac{M_{\odot} r^{3}}{M_{\leftmoon} a_{\odot}^{3}}, \qquad \frac{\Delta a_{NI}}{a_{Kep}} \sim \frac{n_{\leftmoon}^{2} r^{3}}{\mathcal{G} M_{\leftmoon}} = \frac{(M_{\oplus} + M_{\leftmoon}) r^{3}}{M_{\leftmoon} a_{\oplus}^{3}}$$

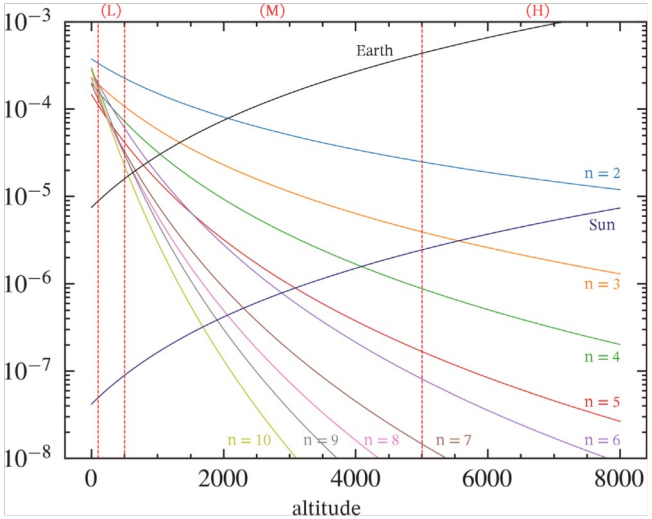
Altitude zones for the characterization of secular dynamics (E. Legnaro & C.E. 2024)

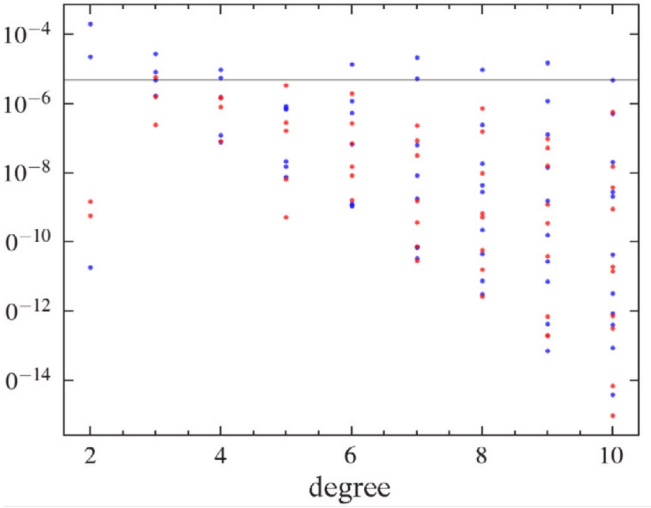
Zone of essentially non-secular dynamics (altitude $a - r_L$ < 100 km): Lunar mascons dominate, no tractable secular force model.

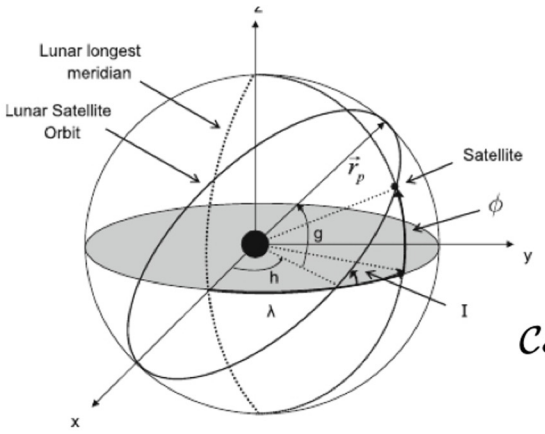
Low Altitude Zone of essentially secular dynamics (altitude 100 km ≤ $a - r_L$ < 500 km): semi-major axis variations ~ 10^{-3}, (two orders of magnitude smaller than those required for re-entry. Cumulative effect of various harmonics of degree $n \leq 10$ (total lunar gravity force perturbation about two orders of magnitude larger than the one due to the Earth's tide).

Middle Altitude Zone of essentially secular dynamics (altitude 500 km ≤ $a - r_L$ ≤ 5000 km): near the lower limit of this zone the lunar multipoles produce a force perturbation superior by more than one order of magnitude to the Earth's tidal perturbation. However, this is reversed at the higher limit, where the problem becomes essentially one perturbed by the Earth plus few harmonics $n = 2$ and $n = 3$.

High Altitude Zone of essentially secular dynamics (altitude $a - r_L$ > 5000 km): any perturbation other than the Earth's tide becomes negligible.







Potential model

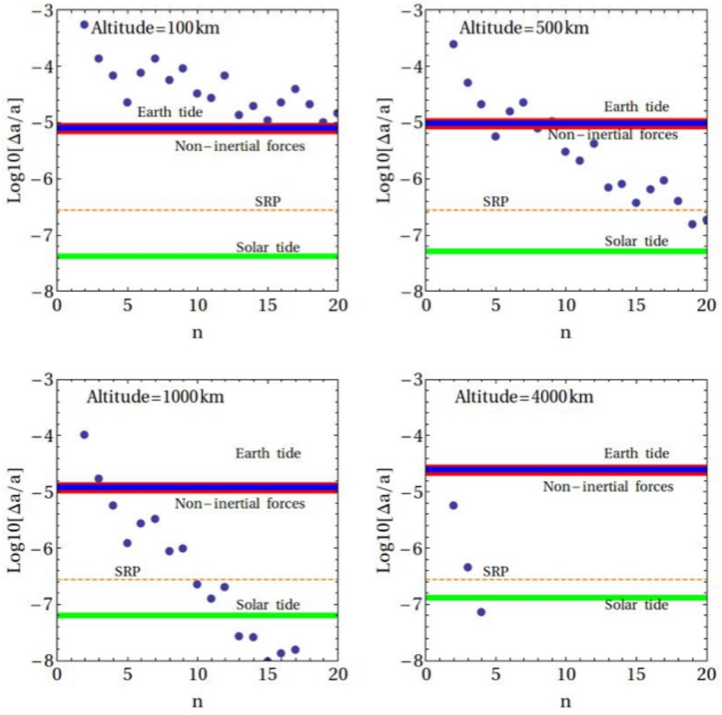
$$V(\mathbf{r},t) = V_{\leftmoon}(\mathbf{r}) + V_{\oplus}(\mathbf{r},t) + V_{\odot}(\mathbf{r},t) + V_{SRP}(\mathbf{r},t)$$

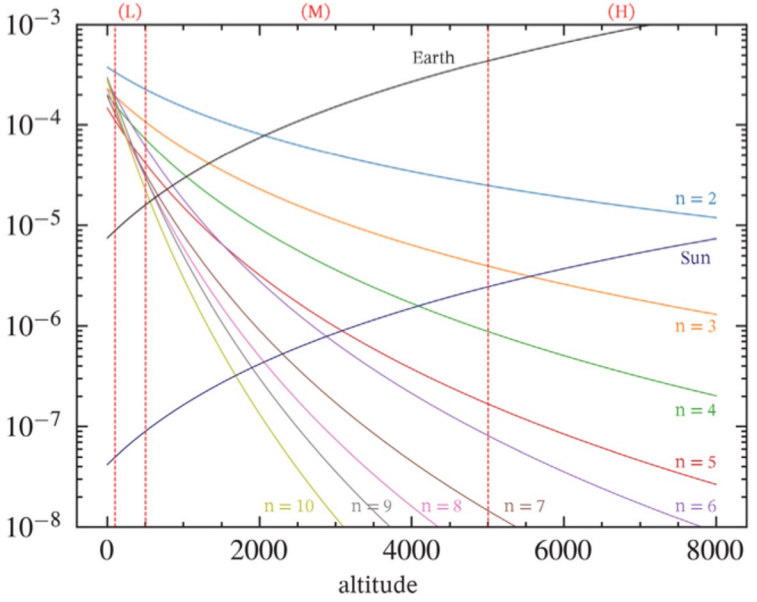
$$\mathcal{CS}_{SSM} = \{C_{20}, C_{22}, C_{30}, C_{31}, S_{31}, C_{40}, C_{41}, C_{60}, C_{70}, C_{71}, C_{80}, C_{90}\}$$

$$V_{\leftmoon}(\mathbf{r}) \simeq V_{\leftmoon}^{SSM}(\mathbf{r}) = -\frac{\mathcal{G}M_{\leftmoon}}{r}\sum_{n=1}^{9}\left(\frac{R_{\leftmoon}}{r}\right)^n \sum_{m=0}^{n} P_{nm}(\sin\phi)[C_{nm}\cos(m\lambda) + S_{nm}\sin(m\lambda)]$$

$$V_{\oplus}(\mathbf{r},t) \simeq V_{\oplus}^{SSM}(\mathbf{r},t) = V_{\oplus,P2}(\mathbf{r},\mathbf{r}_{\oplus}(t)) = \frac{\mathcal{G}M_{\oplus}}{r_{\oplus}(t)}\left(\frac{1}{2}\frac{r^2}{r_{\oplus}^2(t)} - \frac{3}{2}\frac{(\mathbf{r}\cdot\mathbf{r}_{\oplus}(t))^2}{r_{\oplus}^4(t)}\right)$$

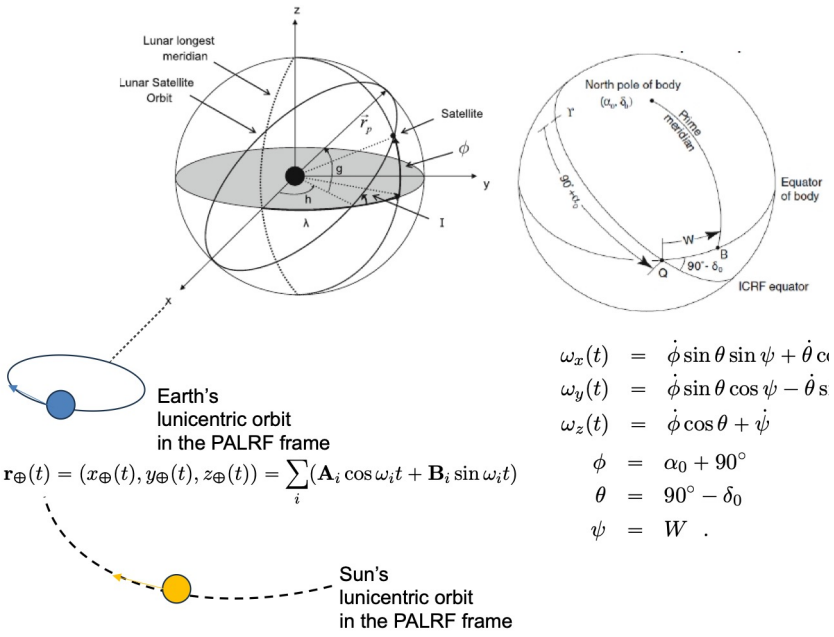
E. Legnaro,M. + C.E. 2024 (Acta Astronautica)





Earth's lunicentric (PALRF) radius vector

SELENA: NAFF model obtained by the INPOP efemeris



$$
\begin{aligned}
\omega_x(t) &= \dot{\phi}\sin\theta\sin\psi + \dot{\theta}\,c\\
\omega_y(t) &= \dot{\phi}\sin\theta\cos\psi - \dot{\theta}\,s\\
\omega_z(t) &= \dot{\phi}\cos\theta + \dot{\psi}\\
\phi &= \alpha_0 + 90^\circ\\
\theta &= 90^\circ - \delta_0\\
\psi &= W\ .
\end{aligned}
$$

i	$\omega_i\ [rad/s]$	$A_i^{(x)}\ [km]$	$B_i^{(x)}\ [km]$	i	$\omega_i\ [rad/s]$	$A_i^{(x)}\ [km]$	$B_i^{(x)}\ [km]$
1	0	382469.63	0	26	2.99241e-6	17.11	3.27
2	3.32012e-8	0.99	-1.	27	3.05881e-6	-1.09	14.94
3	6.64022e-8	0.35	3.14	28	4.3729e-6	-2.19	0.97
4	1.76602e-7	-6.71	2.05	29	4.52701e-6	4.05	-7.22
5	1.99097e-7	39.58	1.25	30	4.572e-6	-24.13	9.49
6	3.53204e-7	-189.3	128.62	31	4.7261e-6	90.03	-145.28
7	3.98194e-7	2.13	0.18	32	4.9252e-6	1369.26	-2010.23
8	4.19607e-7	-35.43	-41.03	33	5.07931e-6	0.35	8.3
9	5.52301e-7	-7.12	4.4	34	5.1018e-6	-1.84	5.93
10	6.18704e-7	-1.38	-1.75	35	5.1243e-6	-10.26	13.76
11	1.8878e-6	1.29	4.59	36	5.27841e-6	-0.75	584.51
12	1.93279e-6	0.81	-1.86	37	5.34481e-6	-1285.72	148.03
13	2.0869e-6	34.53	146.51	38	5.4775e-6	0.27	-6.03
14	2.2196e-6	-11.79	0.86	39	7.0121e-6	1.54	0.59
15	2.286e-6	730.56	3836.11	40	7.2112e-6	12.92	5.64
16	2.44011e-6	41.09	37.63	41	7.36531e-6	5.61	-1.31
17	2.4626e-6	50.8	95.97	42	7.3878e-6	3.07	0.35
18	2.4851e-6	-1.39	-9.46	43	7.5644e-6	71.25	-13.41
19	2.57282e-6	1.32	-1.06	44	7.63081e-6	2.26	7.26
20	2.6392e-6	14796.88	14794.17	45	7.91761e-6	16.81	-16.75
21	2.6617e-6	-6.98	-14.67	46	7.98401e-6	28.08	22.31
22	2.6724e-6	16.34	-0.81	47	9.8504e-6	-1.79	-4.57
23	2.68417e-6	-0.22	-2.32	48	0.0000102036	-5.36	-3.67
24	2.70561e-6	-24.25	30.57	49	0.00001027	1.19	-2.26
25	2.8383e-6	-17.17	-18.66	50	0.0000106232	-0.17	-1.46

Table 1: The Fourier decomposition of the x-coordinate of Earth's position in the Moon's principal axis frame.

Earth's lunicentric (PALRF) radius vector

Earth's radius vector model containing all terms responsible for secular resonances

$$
\begin{aligned}
x_\oplus(t) &= x_\oplus(\varphi_1(t), \varphi_2(t), \varphi_3(t), \varphi_4(t)) \\
&= C_1^{(x)} - C_{15}^{(x)} \cos(\varphi_1 + \varphi_2 - 2\varphi_4) + C_{20}^{(x)} \cos(\varphi_1 - \varphi_2) \\
&+ C_{32}^{(x)} \cos(2\varphi_1 - 2\varphi_4) + C_{37}^{(x)} \cos(2\varphi_1 - 2\varphi_3)\,,
\end{aligned}
$$

$$
\begin{aligned}
\varphi_1 &= \varphi_{1,0} + \dot{\lambda}_{\leftmoon}\, t \\
\varphi_2 &= \varphi_{2,0} + \dot{\varpi}_{\leftmoon}\, t \\
\varphi_3 &= \varphi_{3,0} + \dot{h}_{\leftmoon}\, t \\
\varphi_4 &= \varphi_{4,0} + \dot{\ell}_{\odot} t
\end{aligned}
$$

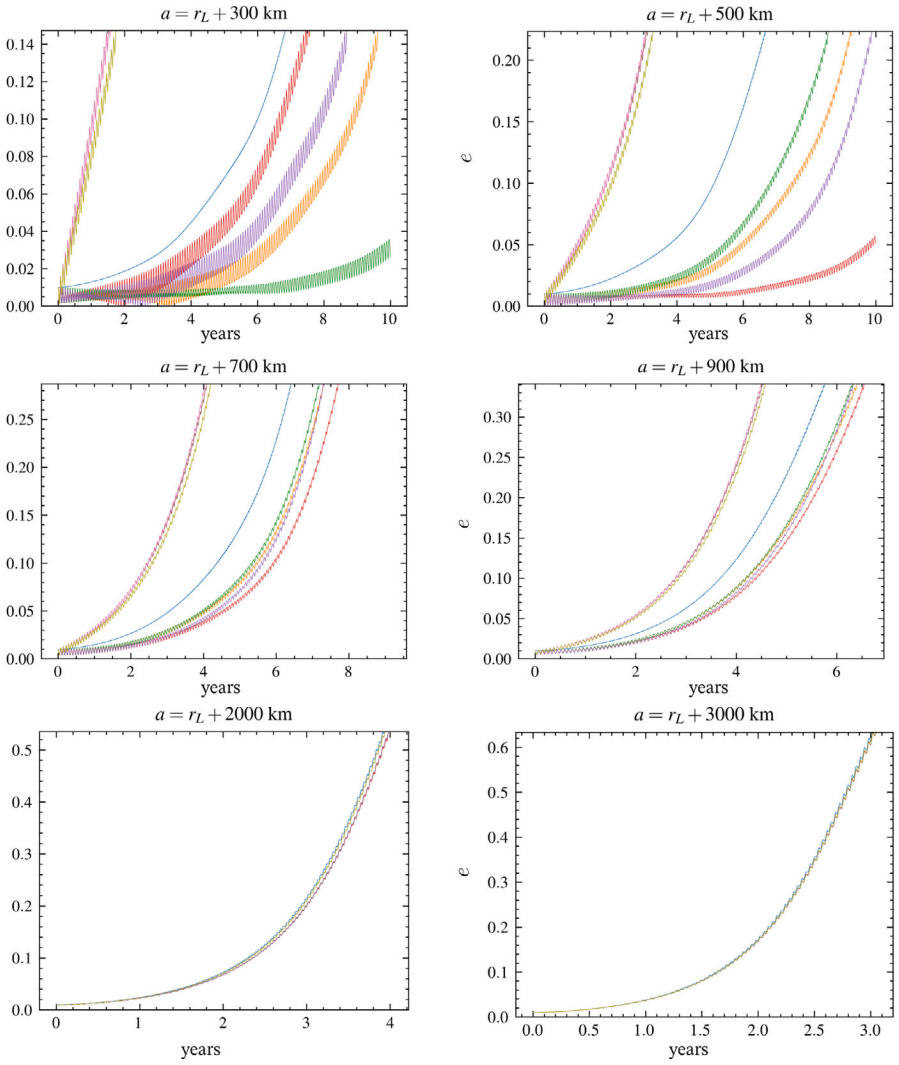
$$
\begin{aligned}
y_\oplus(t) &= y_\oplus(\varphi_1(t), \varphi_2(t), \varphi_3(t), \varphi_4(t)) \\
&= C_8^{(y)} \cos(\varphi_4) + C_{19}^{(y)} \sin(\varphi_1 + \varphi_2 - 2\varphi_4) \\
&- C_{23}^{(y)} \sin(\varphi_1 - \varphi_2) - C_{34}^{(y)} \sin(2\varphi_1 - 2\varphi_4) - C_{39}^{(y)} \sin(2\varphi_1 - 2\varphi_3)\,,
\end{aligned}
$$

$$
\begin{aligned}
z_\oplus(t) &= z_\oplus(\varphi_1(t), \varphi_2(t), \varphi_3(t), \varphi_4(t)) \\
&= -C_5^{(z)} \sin(\varphi_2 - \varphi_3) + C_{15}^{(z)} \sin(\varphi_1 + \varphi_3 - 2\varphi_4) - C_{23}^{(z)} \sin(\varphi_1 - \varphi_3)
\end{aligned}
$$

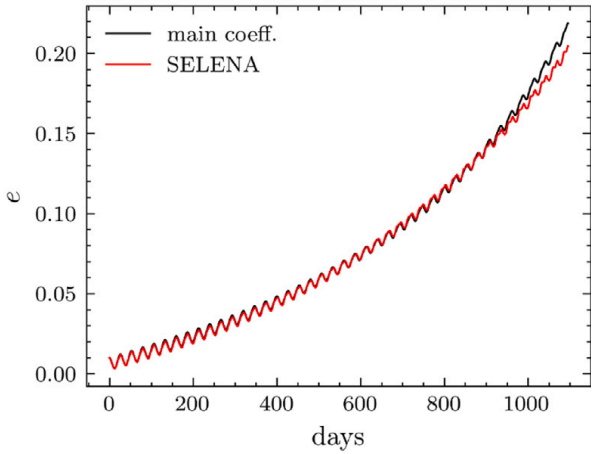
Amplitudes						Initial phases	
$x_\oplus$		$y_\oplus$		$z_\oplus$			
i	$C_i^{(x)}$ [km]	i	$C_i^{(y)}$ [km]	i	$C_i^{(z)}$ [km]	j	$\varphi_{j,0}$ [rad]
1	382469.63	8	1404.92	5	3877.95	1	−1.12751856
15	3905.06	19	8556.95	15	1354.18	2	−0.34221198
20	20924.03	23	42089.48	23	44722.44	3	−2.75562949
32	2432.26	34	3948.49			4	1.52765585
37	1294.21	39	1296.27				

$$
\begin{aligned}
\dot{\varphi}_1 &= \dot{\lambda}_{\leftmoon} = 2\pi/(27.322) = 0.229968 \text{ [rad/days]} \\
\dot{\varphi}_2 &= \dot{\varpi}_{\leftmoon} = 2\pi/(8.84 \cdot 365.26) = 0.0019443 \text{ [rad/days]} \\
\dot{\varphi}_3 &= \dot{h}_{\leftmoon} = -2\pi/(18.6 \cdot 365.26) = -0.000924193 \text{ [rad/days]} \\
\dot{\varphi}_4 &= \dot{\ell}_{\odot} = 2\pi/(365.26) = 0.017202 \text{ [rad/days]}\,.
\end{aligned}
$$

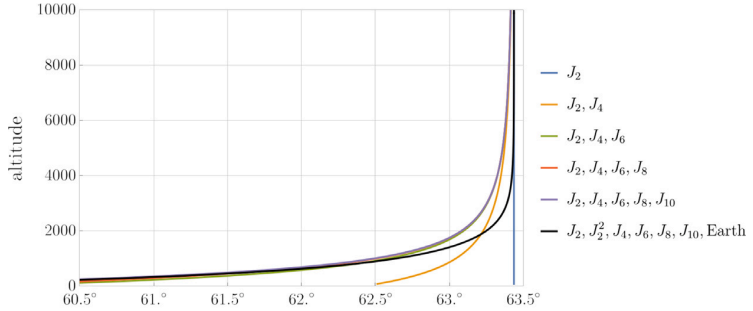
Validation of the simplified secular model (SSM)



Convergence



Comparison with the full grid integration



Position of the critical resonance

Cartography of lunar satellite frozen orbits

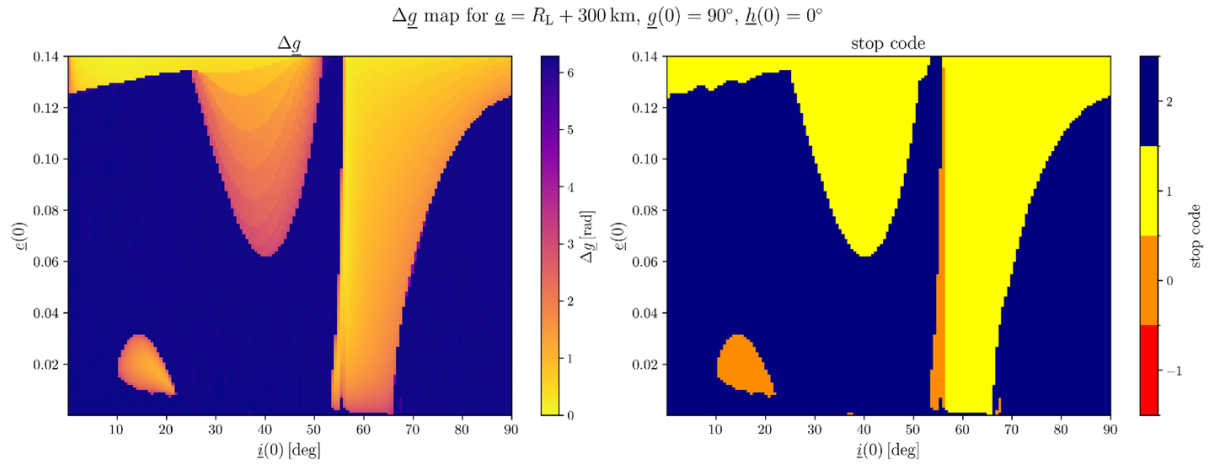


Fig. 9 Numerical survey of frozen-orbit candidates in the $(\underline{i}, \underline{e})$ plane for $\underline{a} = R_{\mathrm{L}} + 300$ km, $\underline{g}(0) = 90°$, and $\underline{h}(0) = 0°$. Left: amplitude $\Delta\underline{g} = \underline{g}_{\max} - \underline{g}_{\min}$; right: stop-code classification of the orbital behavior

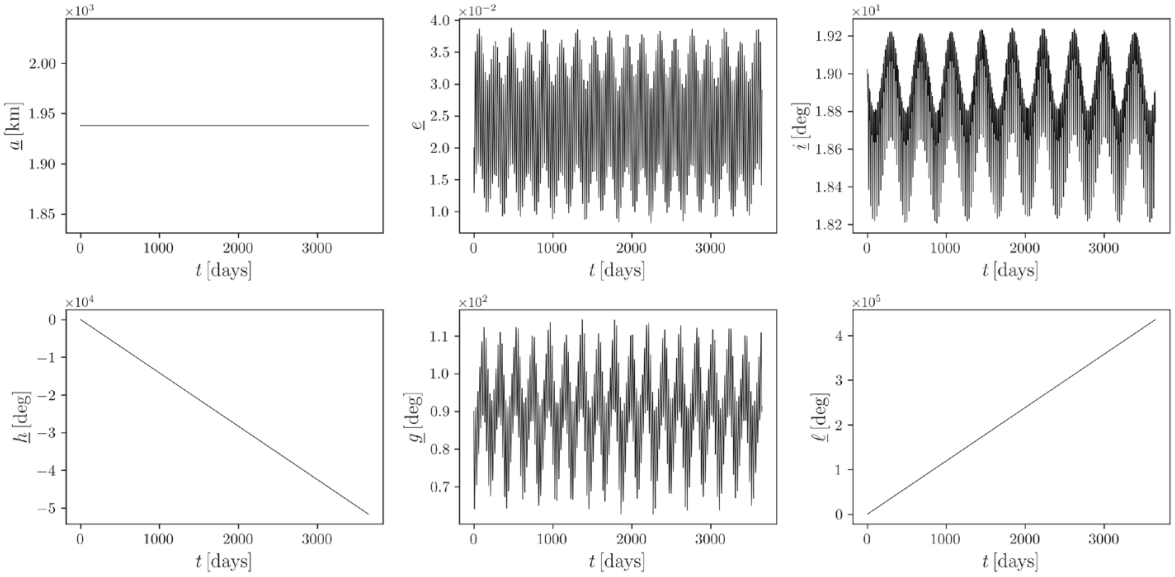
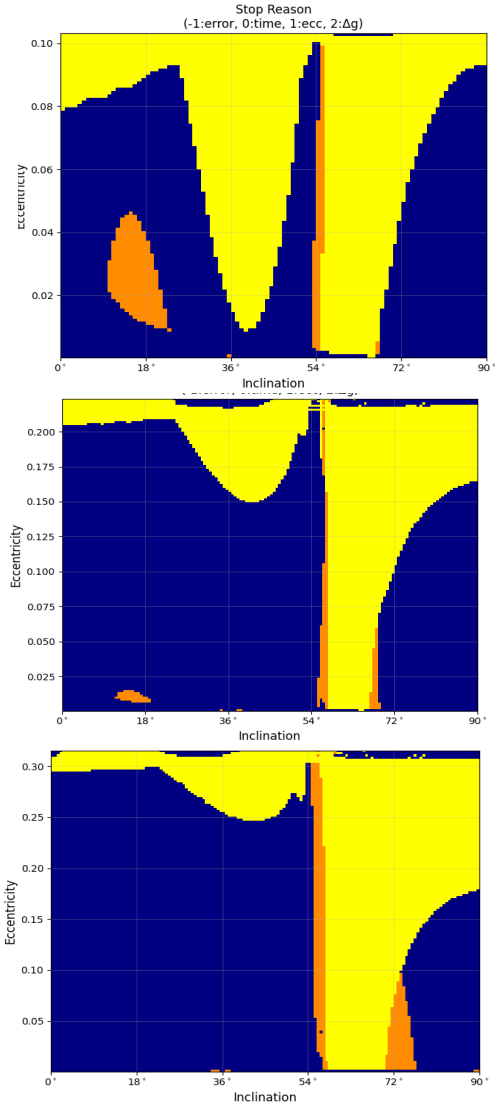


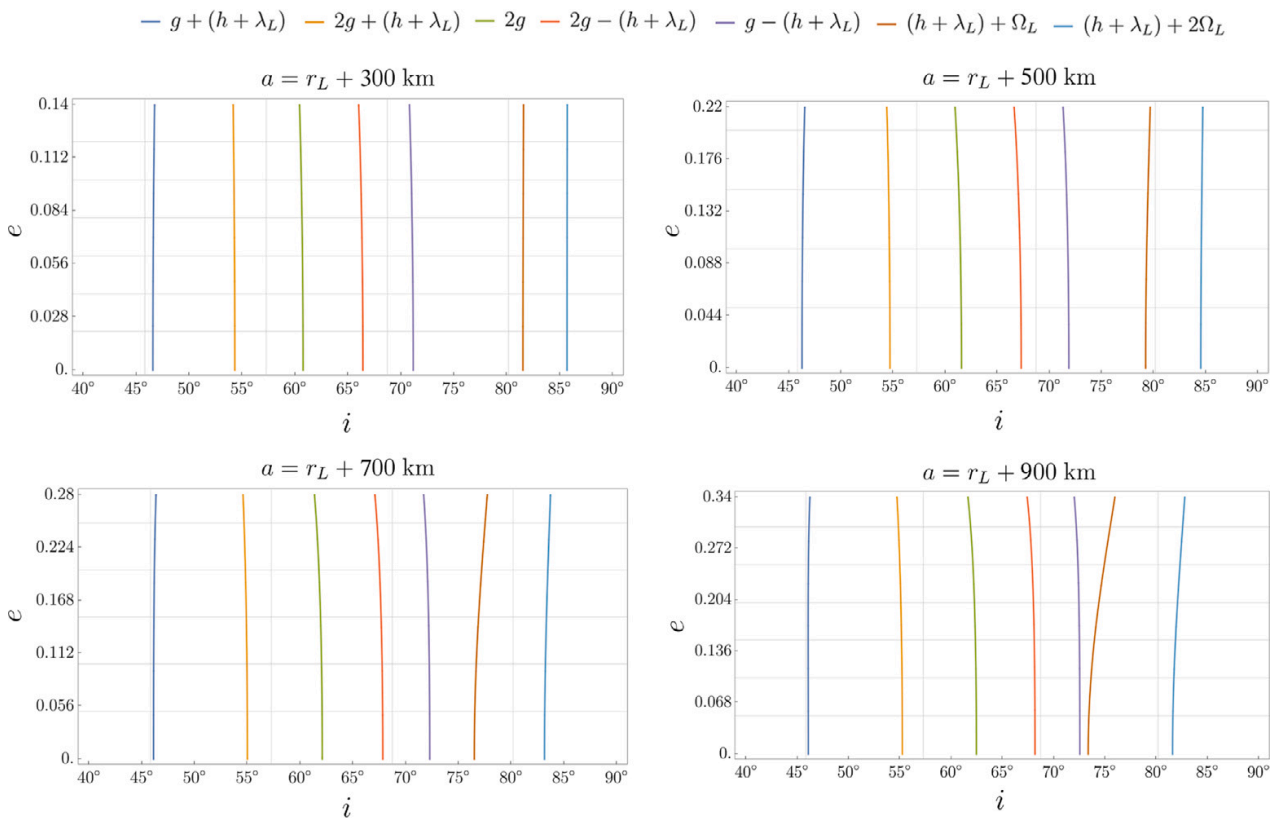
Fig. 10 Secular evolution over 10 years of a frozen orbit with $\underline{a} = R_{\mathrm{L}} + 200$ km and initial mean elements $\underline{e}(0) = 0.02$, $\underline{i}(0) = 19°$, $\underline{g}(0) = 90°$, $\underline{\ell}(0) = 0°$, $\underline{h}(0) = 0°$



Altitude: 200, 500, 800 km

Most theoretical frozen orbits found in literature under truncated secular models, or simplified models of the evolution of the Earth's radius vector, cease to exist in the integration under a more complete model (cf. *Giacaglia et al. (1970); Kneževic and Milani (1998), Elipe and Lara (2003), De Saedeleer (2006), Lara et al. (2009a,b)*).

Main contributor to the phenomenon: the **structure of secular resonances**

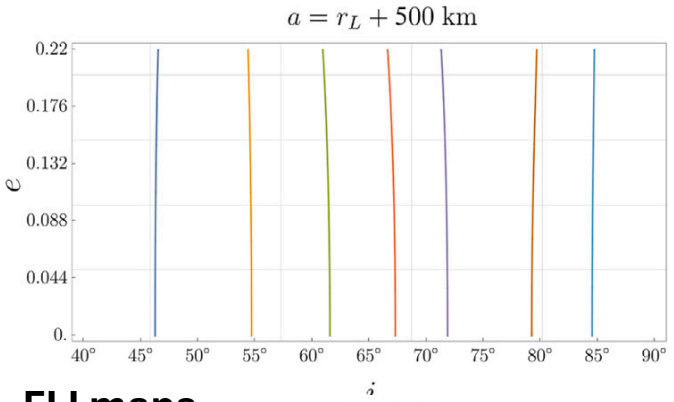


The even zonal harmonics define the centers of the resonances'. H_0 contains contributions from the even degree zonal harmonics (J_2,J_4,...), as well as from the Earth's tidal potential, (of relative importance $((\mu E/\mu L)(a/RL)^2$ $(a/aL)^3)$ with respect to the $J2$ term, i.e. negligible). Thus, the locations of all resonances are determined, practically, by the even zonal harmonics J_{2j}, j = 1,2,....

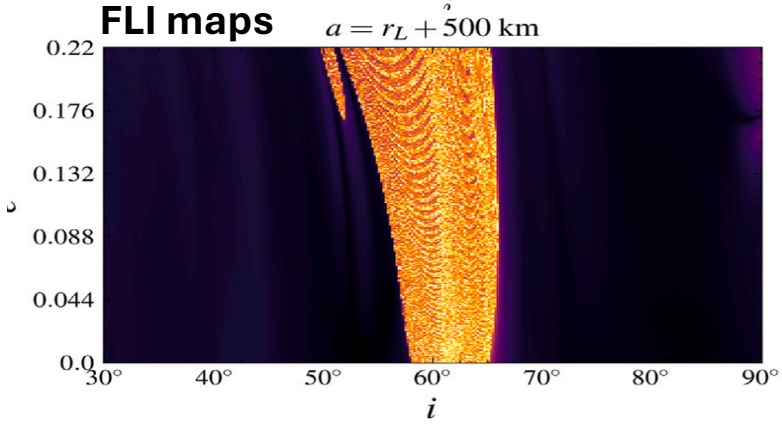
'The form of the separatrices of the $2g$-resonance, are determined by all zonal harmonics J_n, n = 3,4... and by the Earth's tidal term. The J_2 term contributes no trigonometric term to the Hamiltonian H_1. The remaining even zonal harmonics $2j > 2$ all contribute a first order $O(J_{2j}R_L{}^{2j}e^2/a^{2j+1})$ $\cos(2g)$ term to H_1. Odd zonal harmonics J_{2j+1}, j = 1,2,...contribute to odd trigonometric terms $e\sin(g)$,$e^3\sin(3g)$, etc, with the same scaling. The Earth's potential contributes a $O(e^2\mu_E(a/a_L)^3)$ $\cos(2g)$ to to H_1.

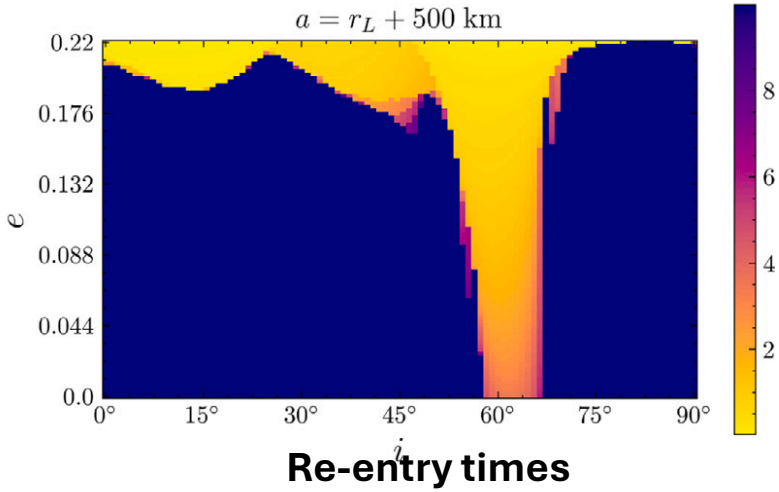
The form of the separatrices of all secular resonances of the form $k_1g + k_2(h + \lambda_L)$ with $k_2 \neq 0$ is determined only by terms of the Earth's tidal potential proportional to $\sin(\varepsilon_L)$, where $\varepsilon_L \simeq 0.12$ rad is the Moon's obliquity. Tesseral harmonics Cn,m, Sn,m, with $n \geq 2$, $1 \leq m \leq n$, do not contribute to H_0, while they appear in H_1 through the satellite's longitude of the nodes h, but not through the slow angle $h + \lambda_L$.

Trigonometric terms in H_1 depending on the angle Ω_L are produced only by the Earth's tidal potential, and they are of order $O(e^2\mu_E(a/a_L)^3)$ $\sin(\varepsilon_L)$ $\sin(i_p)$, where $i_L \simeq 0.09$ rad is the inclination of the Moon's orbit with respect to the ecliptic.



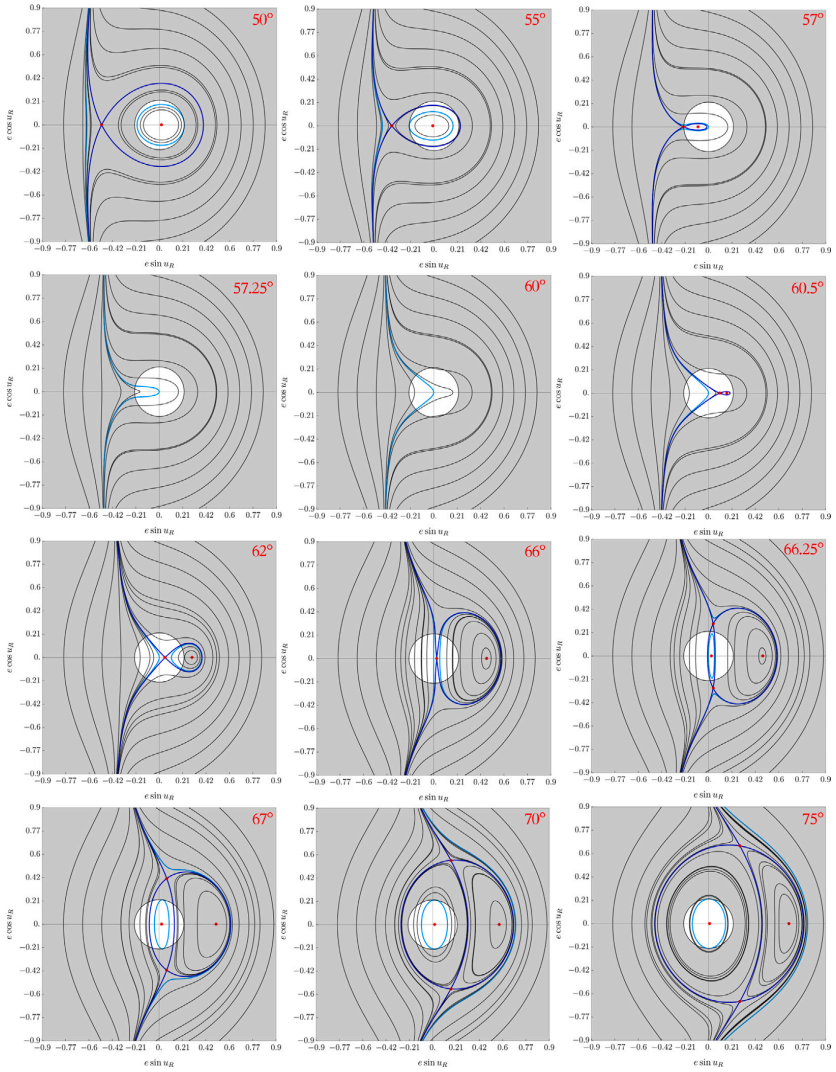
FLI maps





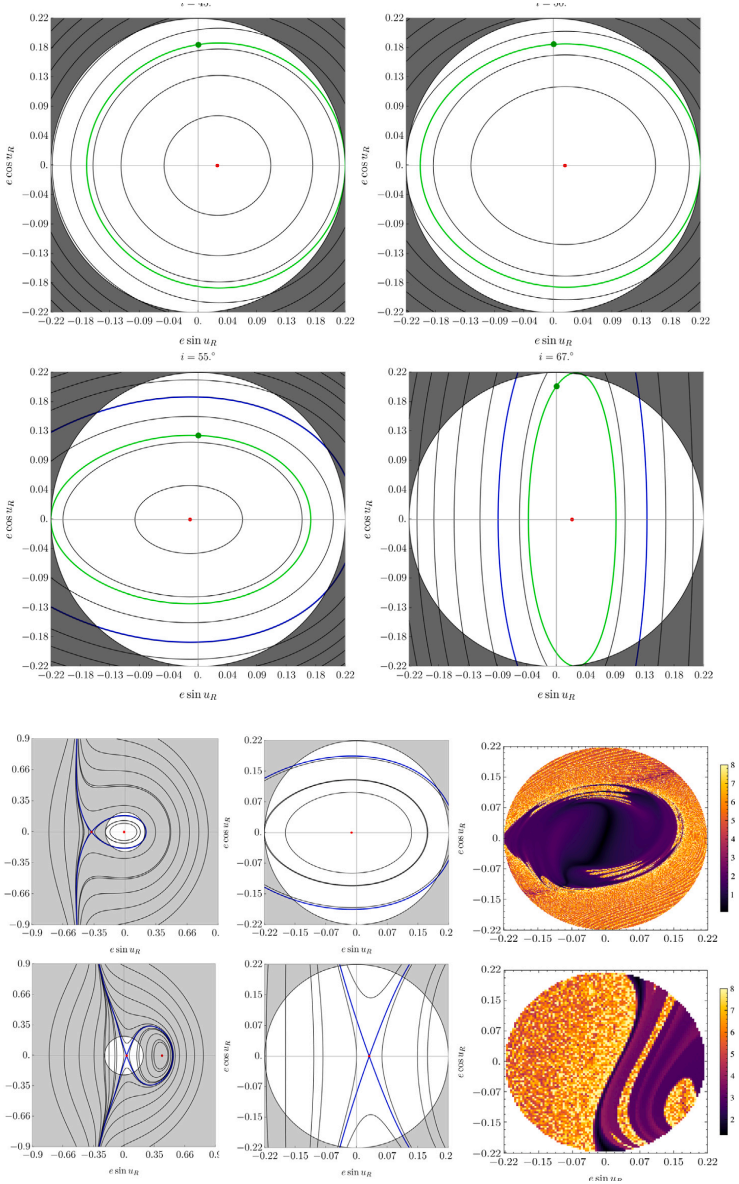
Re-entry times

Resonant phase portraits (a-r_L=500 km)

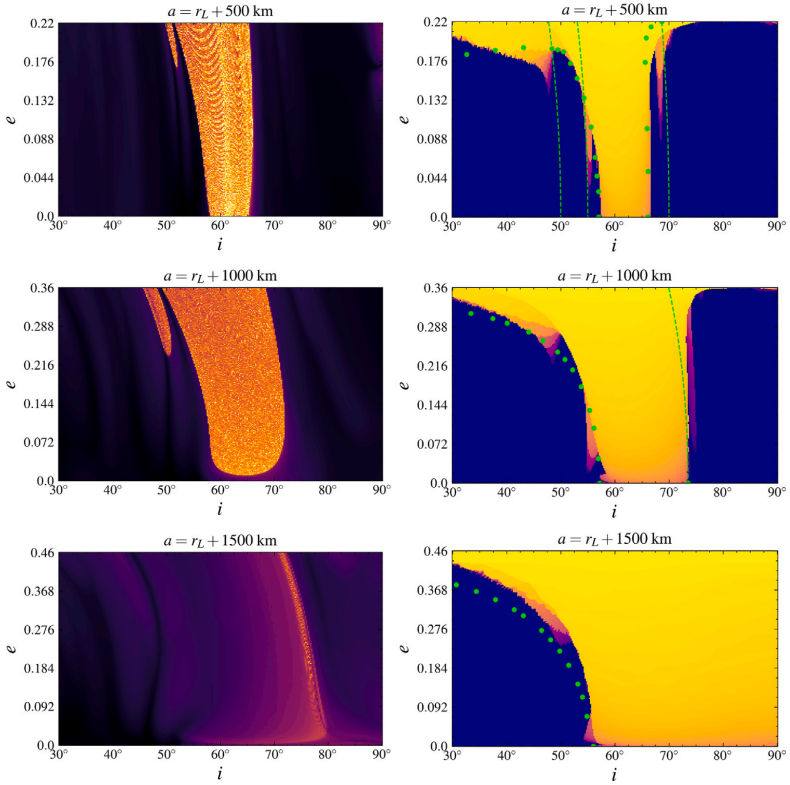


E. Legnaro,M. + C.E.2024 (Acta Astronautica)

Theoretical re-entry limits

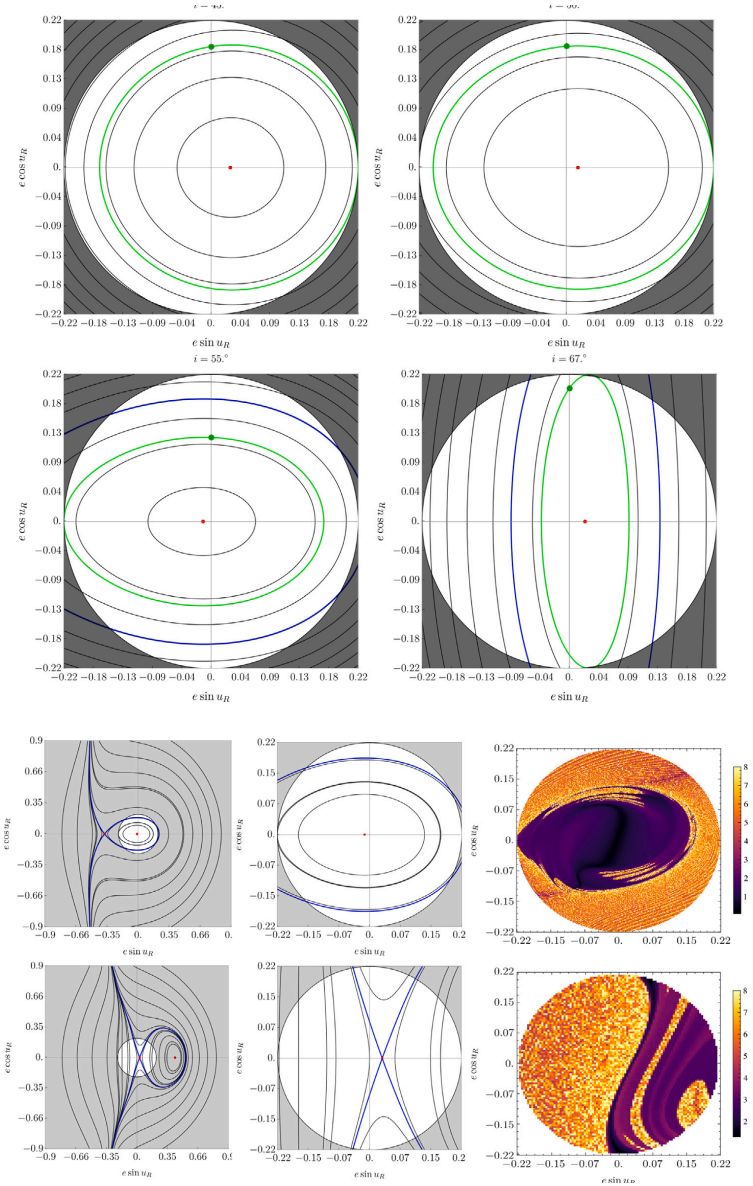


Predictions vs numerical re-entry limits

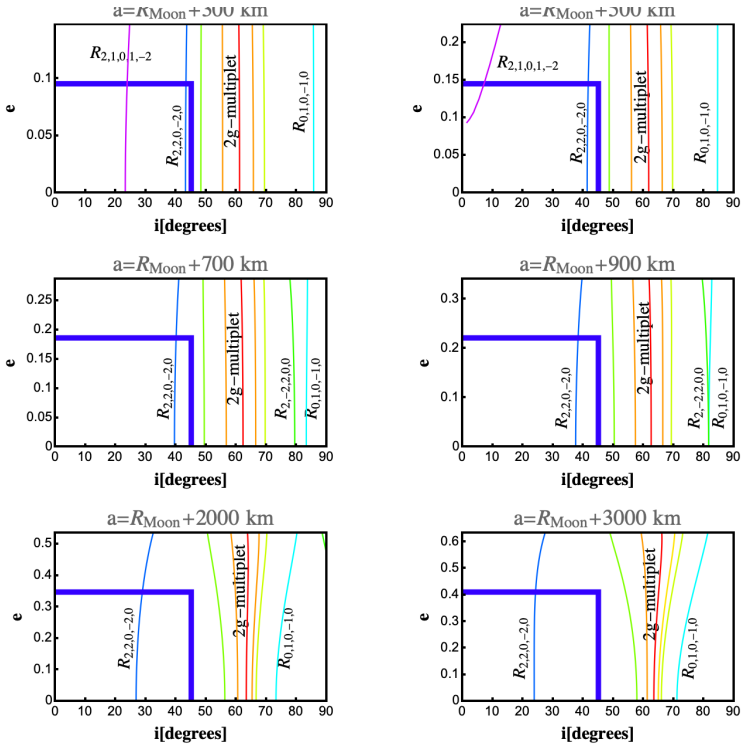


E. Legnaro,M. + C.E. 2024 (Acta Astronautica)

Theoretical re-entry limits



Secular dynamics and resonances



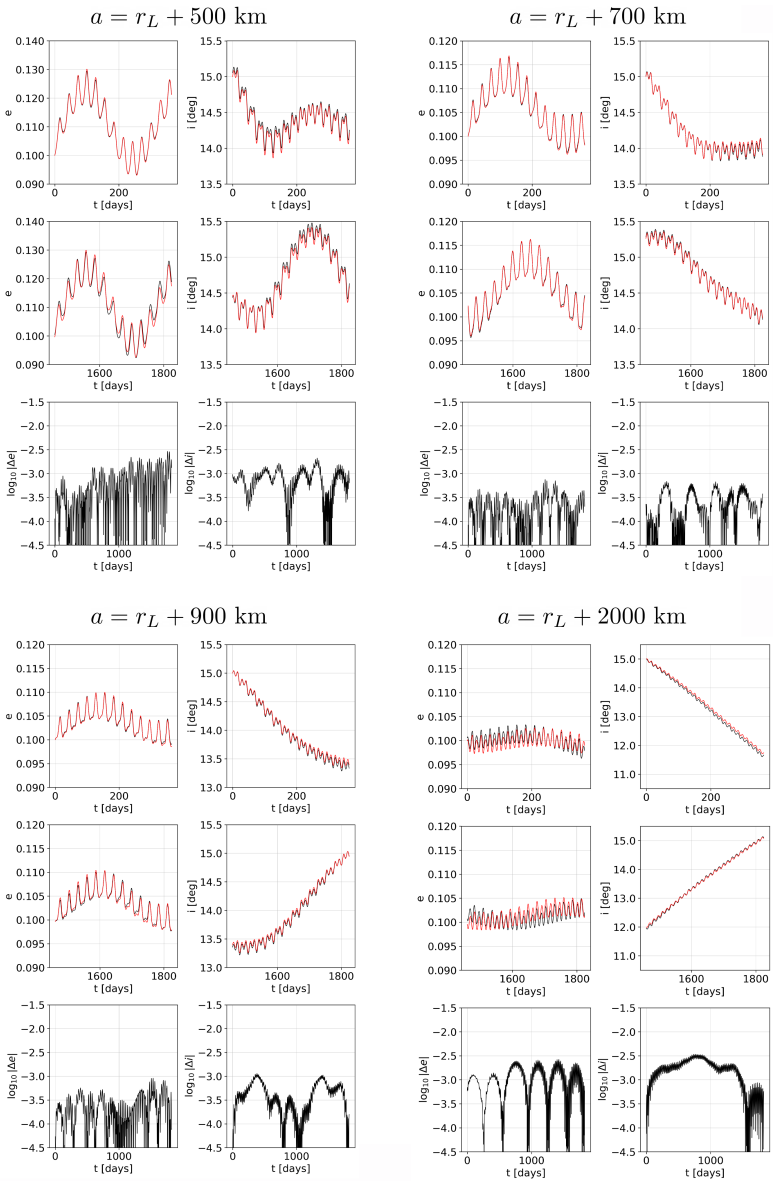


Fig. 6: The curves $e_p(i_p)$ of all the dynamically important resonances for prograde orbits ($i < 90°$) and for the set of values of the semi-major axis $a_p = \underline{a} = R_{\leftmoon} + \delta a$ with $\delta a = 300$, 500, 700, 900, 2000, 3000 km. The limits in eccentricity in each plot is $0 \le e_p \le \delta a/\underline{a}$, same as in Figure 5 of [1]. The parallelogram with thick blue border indicates the limits of the corresponding panels in Figs. 1 and 2 of the present paper. The parallelogram is crossed by the resonances $\mathcal{R}_{2,1,0,1,-2}$ (resonant angle: $2g+\widetilde{\Omega}+h_{\leftmoon} - 2\ell_\odot$, purple), for $a_p = R_{\leftmoon} + 300$ km and $a_p = R_{\leftmoon} + 500$ km, and $\mathcal{R}_{2,2,-2,0,0}$ (resonant angle: $2g+2\widetilde{\Omega}-2\varpi_{\leftmoon}$, blue), for the entire set of values of a_p. The corresponding curves compare well with the centers of the narrow yellow strips found in the panels of equal value of the semi-major axis shown in Figs. 1 and 2. Outside the parallelogram, at all values of the semi-major axis, we have the bundle of resonances collectively referred to as '2g-multiplet', with the '2g-resonance' ($\mathcal{R}_{2,0,0,0,0}$, red) in the center, and the resonances $2g + (\widetilde{\Omega} - h_{\leftmoon})$ (first left), $2g - (\widetilde{\Omega} - h_{\leftmoon})$ (first right), $2g + 2(\widetilde{\Omega} - h_{\leftmoon})$ (second left), $2g - 2(\widetilde{\Omega} - h_{\leftmoon})$ (second right). Finally, in the domain of polar orbits we have the secular resonance $\widetilde{\Omega} - h_{\leftmoon}$ ($\mathcal{R}_{0,1,0,-1,0}$), which appears at inclinations near 90° at low altitudes and approaches to the 2g-multiplet as the altitude increases, as well as the transient resonance $2g - 2\widetilde{\Omega} + 2\varpi_{\leftmoon}$ (i.e. $\mathcal{R}_{2,-2,2,0,0}$, which appears at the altitude 700km and disappears at the altitude $\sim$ 2000km.)

Summary

1. Frozen orbits are produced either near the forced equilibria of zonal potential perturbations beyond J2, or by the Lidov-Kozai mechanism (near the critical inclination for the 2g-resonance). In the latter case, the mechanism can be activated either by even zonal harmonics or by third-body tidal perturbations.

2. In the moon's case, lunar mascons affect mostly the Moon's zonal harmonics, hence the produce separatrices which are highly distorted/topologically different from the figure-8 separatrices of the symmetric Lidov-Kozai phase portrait of the 2g-resonance applicable in simpler cases (e.g. for Earth satellites).

3. (1) and (2) above, combined with the Earth's synchronous rotation around the Moon, imply that no other secular resonance is important in the phase space, except for the 2g-resonance or multiplets thereof involving the slow frequencies of the Earth's lunicentric radius vector. Such multiplets accumulate also around near-polar orbits.

4. Due to (1), (2), and (3) above, frozen orbits are obuiquitous around the forced equilibria created by odd zonal harmonics, and way less obuiquitous around the stable equilibria of the 2g-resonance, or around polar orbits. Many of the orbits found in simplified or highly truncated secular models stop to exist when more complete models of the gravity and of the evolution of the Earth's lunicentric radius vector are considered.